Heatwaves in Europe: Areas of homogeneous variability and links with the regional to large-scale atmospheric and SSTs anomalies

Carril Andrea F., Gualdi Silvio, Cherchi Annalisa and Navarra Antonio

Istituto Nazionale di Geofisica e Vulcanologia, INGV

Centro Euro-Mediterraneo per i Cambiamenti Climatici, CMCC

May 2007,

Climate Dynamics, in press

Corresponding author: Dr. Andrea F. Carril

carril@bo.ingv.it

INGV-CMCC, Via Donato Creti 12, 40128, Bologna, Italy

Ph. (direct): +39 051 415 14 37

Fax: +39 051 415 14 99

Abstract

This work presents a methodology to study the interannual variability associated with summertime months in which extremely hot temperatures are frequent. Daily timeseries of maximum and minimum temperature fields (T_{max} and T_{min} respectively) are used to define indexes of extreme months based on the number of days crossing thresholds. An empirical orthogonal function (EOF) analysis is applied to the monthly indexes. EOF loadings give information about the geographical areas where the number of days per month with extreme temperatures has the largest variability. Correlations between the EOF principal components and the time series of other fields allow plotting maps highlighting the anomalies in the large scale circulation and in the SSTs that are associated with the occurrence of extreme events. The methodology is used to construct the "climatology" of the extremely hot summertime months over Europe. In terms of both interannual and intraseasonal variability, there are three regions in which the frequence of the extremely hot days per month homogeneously varies: north-west Europe, Euro-Mediterranean and Eurasia region. Although extremes over those regions occur during the whole summer (June to August), the anomalous climatic conditions associated with frequent heatwaves present some intraseasonal variability.

Extreme climate events over the north-west Europe and Eurasia are typically related to the occurrence of blocking situations. The intraseasonal variability of those patterns is related to the amplitude of the blocking, the relative location of the action centre and the wavetrain of anomalies downstream or upstream of the blocking. During June and July, blocking situations which give extremely hot climate conditions over north-west Europe are also associated with cold conditions over the eastern Mediterranean sector. The Euro-Mediterranean region is a transition area in which extratropical and tropical systems compete, influencing the occurrence of climate events: blockings tend to be related to extremely hot months during June while baroclinic anomalies dominate the variability of the climate events in July and August.

We highlight that our method could be easily applied to other regions of the world, to other fields as well as to model outputs to assess, e.g., the potential change of extreme climate events in a warmer climate.

Key words: extreme events, heatwaves, temperature variability, climate variability

1. Introduction

As Europe is warming up (e.g., Jones and Moberg 2003, Giorgi 2002), there is evidences that extreme events might become more frequent and intense (Klein Tank and Können 2003, IPCC 2001, Easterling et. al 2000). The summer decade 1994-2003 has been the warmest period in Europe during the 20th century and the summer of 2003 has been the warmest summer since 1500 (Luterbacher et al., 2004). Moreover, some studies have documented an increase in the average frequency of heat waves of 0.24 per decade since 1880 (Della-Marta et al. 2007) while others, have reported the increase (decrease) of warm (cold) extremes during the last 40 years (Klein Tank and Können 2003, Yan et al. 2002). Some authors claim that extremes such as those recorded during the summer of 2003 do not fit into the statistics spanned by the observations of the last decades. Nevertheless, model simulations indicate that extraordinary hot summers could become more frequent in a warmer climate, when relevant changes in the variance of the temperature distribution are expected (Beniston 2004, Schär et al. 2004, Stott et al. 2004,).

Some studies relate the heatwaves to blockings in the extratropical circulation, altering the pattern of horizontal advections, warming the atmospheric surface levels due to adiabatic heating by subsidence and enhancing the solar radiative heating (e.g., Della-Marta et al. 2007, Beniston and Diaz 2004, Black et al. 2004, Fink et al. 2004, Xoplaki et al. 2003b). However, we know that summertime climate in the Euro-Mediterranean region is dominated by the alternation of extratropical weather regimes and subsidence of tropical-dry air by the descending branch of the Hadley cell (Bolle 2002). Moreover, in terms of pressure and temperature anomalies, there is an anti-phase relationship between the eastern and western Mediterranean (Corte-Real et. al 1995). Therefore, the thesis that extratropical blockings are a dominant mechanism associated with the occurrence of extreme conditions could be questionable and the issue of how far the exceptional heatwaves can be explained by anomalous and persistent blocking conditions remains to be addressed.

A relevant issue concerns the temporal scales. Many authors have analyzed the anomalies observed during the 2003 summer heatwave following different approaches (e.g., Cassou et al. 2005, Ogi et al. 2005, Nakamura et al. 2005, Trigo et al. 2005, Black et al. 2004, Beniston 2004, Beniston and Diaz 2004, Fink et al. 2004, Schär et al. 2004). From these studies it turns out that the anomalous temperature pattern of the heatwave is strongly dependent on the timescale considered for the analysis. While the mean summertime temperature anomaly, covering a vast area centered over France, exceeded 4°C (Fig. 1 in Schär et al. 2004), the largest monthly mean anomaly (of about

5°C) occurred over the Euro-Mediterranean region in June and over southern France, Switzerland and south-west Germany in August (Fig. 1 in Fink et al. 2004). Moreover, a considerable different picture emerges when the August 2003 heatwave is analyzed in sub-monthly timescale: maximum anomalies of about 10°C peaked over north-western France during the first fortnight of August (Fig. 1b in Trigo et al. 2005).

In this work, our challenge is to classify extreme months and to explore the potential links between frequent occurrence of extreme weather conditions over Europe and anomalous large scale patterns. To this aim we define a methodology able to identify and characterize the occurrence of these episodes. The work is organized as follows. In Section 2 the datasets and the methodology are described. Section 3 introduces the areas of homogeneous extreme variability and the associated large scale anomalies in atmospheric fields and SSTs. Discussion considers the differences between extremes in T_{max} and T_{min}, as well as the intraseasonal variability of the patterns. In section 4 our method is tested by reconstructing the 2003 European heatwave; composites illustrating a 2003-like heatwave are displayed. Discussion and conclusions are presented in Sections 5 and 6, respectively.

2. Data and Methodology

Based on the "European Climate Assessment daily dataset" (ECA, Klein Tank et al. 2002), the European scientific community (as a task of the European Union project ENSEMBLES, GOCE-CT-2003-505539) is concentrating efforts to build a consistent and homogeneous station dataset for climate studies purposes. Although a good practice is the selection of extremes from station data, while waiting for the homogenization of the European station dataset, our approach to explore into the potential links between extremes in temperature and the large-scale anomalous regimes is implemented using NCEP reanalysis (Kalnay et al. 1996). We do not intend to address the question of how well the reanalysis compares with the 2-metre temperature in station data. We know a priori that the description of extremes in temperature is more accurate in station data than in reanalysis datasets. Nevertheless, from a continental perspective, there is a reasonable degree of confidence in the quality of the reanalysis, and we trust we can get some insights into the problem of scale-interactions. There are several antecedents in literature about approaching heatwaves starting from daily temperature series obtained from reanalysis (e.g., Trigo et al. 2005, Nakamura et al. 2005, Black et al. 2004, Xoplaki et al. 2003b).

In our analysis we investigate extreme climate conditions over Europe. These are defined as months during which a large number of extreme days occur. In other words, we study "extreme climate events" and their interannual variability (hereafter, simply "extreme events"). Moreover, our analysis is applied to the summertime months June, July and August separately, to explore the potential intraseasonal variability related to the occurrence of heatwaves (as suggested by Cassou et al. 2005). We have also discriminated between extremes occurring in T_{max} and T_{min} because diurnal extreme temperatures are not necessarily related to the same physical processes as extremes in nocturnal cooling.

Extreme events we have been defined starting from daily time series of T_{max} (T_{min}), linearly detrended, and covering the whole European domain (30°N-60°N, 10°W-50°E). Those time series are used to build a monthly dataset with information about the number of extreme days registered month per month and year per year, at every grid point of the European domain. Specifically, starting from T_{max} (T_{min}) series (daily data) we have built monthly series of extreme days (monthly data). The possible range of values for the monthly series is 0-30 (31), representing the number of extreme days registered in a particular month.

An important step at this point is how to define extreme days, since the approach adopted could affect the interpretation of the relative impact of specific events (e.g., Beniston and Stephenson 2004). In our analysis we use a non-parametric method based on the threshold approach (IPCC 2001). A certain day becomes an "extreme-day" when T_{max} (T_{min}) goes beyond the 75% quantile. Only those days in which T_{max} (T_{min}) exceeds the score of the 75^{th} percentile are counted to build the series representative of the extreme months. We highlight that the score of the 75^{th} percentile is a function of both the grid point and the calendar day (calculated for a 5-day window centered on each calendar day, in the period 1958-2004). Typical values for the 75^{th} percentile score are 0.5 to 1.6. Those scores are anomalies (expressed in degrees) relative to a grid-point and calendar-day mean value. Defining extremes when anomalies are exceeding "variable thresholds" is a particularly useful method because allows a comparison between extremes occurring in different regions and at diverse elevations.

The series of monthly values of extreme days, i.e. how many extreme days occur in a month, is then used to study the characteristics of the extreme climatic conditions over a specific region, in our case the Euro-Mediterranean.

As an example, Figure 1 shows the map of the mean number of extreme days per month for the T_{max} during July. The picture indicates that the number of extreme days is generally higher over the continents, with maxima over the Iberian Peninsula, southern France, northern Italy and the Balcanic Peninsula. Over these regions, in July, the number of extreme days per month is on average about 10. A visual inspection of the series of the monthly values of extreme days (hereafter, for the sake of simplicity, simply EM) reveals a remarkable interannual variability. In other words, for each grid point, the number of extreme days per month exhibits substantial variations from year to year. Interestingly, from the map of EM standard deviation (not shown), the variability appears to be higher over the oceans (North Sea and Mediterranean Sea), where the mean EM has a relative minimum (Figure 1).

In order to investigate the characteristics of the variability of the occurrence of extreme events over the Euro-Mediterranean region, we apply an EOF analysis to the EM time series. The result of this analysis will allow us to identify possible leading modes in the interannual variability of the extreme events.

Since the EOF analysis is used in a frequency domain (the EM fields are spatial distribution of frequency of extreme events), grid points with positive (negative) values of the loadings are characterized by more (less) than average days per month with extreme temperatures. To avoid domain dependent results, varimax rotation is applied (e.g. review article from Richman 1986) and the number of components retained for rotation is determined by the break in the scree plot (Cattell 1966).

After identifying the areas where the extremes maximize, our second goal is to verify whether the occurrence of extreme climate conditions over Europe is associated with specific patterns of the large scale circulation. To this aim we explore the potential link between the occurrence of months with a large number of extreme days and patterns of the large scale circulation and SST anomalies, based on composites and correlation maps. We have inspected the behaviour of diverse fields: skin temperature (SKT), sea level pressure (SLP), high and low-level thickness (500-200 hPa and 1000-500 hPa respectively), outgoing long-wave radiation (OLR), precipitation (PP), zonal anomaly of streamfunction (eddy STM) at low and high-levels (sigma 0.8 and 0.2 respectively), zonal and meridional component of the surface winds (USurf, VSurf), zonal and meridional components of the wind field at 200 hPa (U200, V200), vertical velocity at 500 hPa (Om500) and precipitable water (PRWTR). Most of the fields are taken from the NCEP/NCAR reanalysis (Kalnay et al. 1996, Kistler et al. 2001) for period 1958-2004. OLR and PP are shorter datasets (1979-2004); the interpolated OLR dataset is that provided by NCAR/NOAA (Liebmann and Smith 1996) while the PP dataset is the Xie-Arkin climatology (Xie and Arkin 1997). Non-parametric methods are also used to compute correlations and testing composites. Because linear correlations could be greatly affected by outliers, we have estimated correlations based on the Spearman rank method (e.g., Spiegel and Stephens, 1961). Both, correlation and composite maps are tested at $p<0.05$. The 95% is in general accepted as a good level of significance when studying extremes (e.g., Cassou et al. 2005, Haylock and Goodess 2004, Xoplaki et al. 2003b). Again, to avoid using methods that assume normal distributions (e.g., the t-test), the significance of both correlation and composite maps is determined by a permutation test, generating the reference distribution by Montecarlo sampling.

Previous studies have shown that 2003 heatwave does not fit the present climate statistics (e.g., Schär et al. 2004). For that reason, results in Section 3, illustrating the large scale anomalies associated with the occurrence of extreme warm months, are obtained by analyzing time series in which the year 2003 was removed. After that, in Section 4, we test the ability of our approach to

capture specific extremes, discussing the summer of 2003 as a case study. Results displayed in Section 4 are obtained by analyzing the full time series (i.e., the year 2003 is included).

3. A characterization of extreme months over the Euro-Mediterranean region

We present the classification of the extreme summertime months, based on the frequency of days with temperatures exceeding a threshold. First, patterns of interannual variability of the extreme months in the European domain are introduced. Then, we illustrate the potential links between the occurrence of extreme events and the atmospheric and SST variability, focusing on the intraseasonal variability of the extremes. The analysis is performed by computing the EOF of the EM series over the whole European domain (30°N-60°N; 10°W-50°E). As a first step, we performed the EOF analysis after removing the 2003 from our dataset. The motivation for this choice is to exclude (temporarily) the very extreme year of the 2003, which might affect the entire analysis. This year, in fact, due to its very extreme character (e.g., Luterbacher et al., 2004) might obscure important features of the EM variability occurred during recent decades.

3.1. Areas of homogeneous extreme variability

Figure 2 presents the varimax-rotated EOF leading loadings of the EM time series. Three leading modes mainly contribute to the interannual variability of number of days per month with maximum temperatures in the right tail of the statistical distribution (extreme hot days). Shaded areas highlight those regions in which the loadings are higher than an arbitrary threshold (i.e., regions in which the local variance maximizes).

As displayed in Figure 2, the EM occurrence maximizes over three European sub-domains: the north-west Europe (hereafter NW-EU; Fig. 2, left column), the Euro-Mediterranean sector (Med-EU; Figs. 2, middle column) and the Eurasia region (EU-Asia; Figs. 2, right column). The results obtained for the different summer months, June (panel a, b, c), July (d, e, f) and August (g, h, i) indicates that there are small intraseasonal changes in the patterns. However, a more detailed discussion of the intraseasonal character of the variability will be done in Section 3.2.

When the method is applied to extremes in T_{min} we obtain similar patterns (not shown). The correlation coefficients between the timeseries (PCs) associated with the interannual variability of extreme months in T_{max} and T_{min} for each region are presented in Table 1. High correlations indicate that extremes in T_{max} and T_{min} have a similar behaviour and that, presumably, the climatic anomalies that favour diurnal extremes are similar to those that are associated with the nocturnal

extremes. The results indicate that the correlations are generally high with the exception of the extremes over the Med-EU in July. In this case the behaviour of T_{min} and T_{max} appears to be significantly different (a more detailed discussion is found in Section 3.2).

To assess the capability of the EOF analysis to capture the variability of the extreme events, we have computed correlations between diverse indexes as illustrated in Table 2. There are six panels in the table, each one displaying correlations for a particular month and for extremes in T_{max} (left panels) and T_{min} (right panels). In each panel, the first column indicates the selected area (as illustrated in Fig. 2), the second column displays the correlations between the PCs associated with the selected area and the area-averaged anomaly of EM series (i.e., an index of the extremes frequency, F_a), while the third column illustrates the correlations between the PCs and the box-averaged temperature anomaly (i.e., an index of the temperature field, T_a). The high correlations in the second column denote the success of the EOF approach to capture the interannual variability of the extremes over particular areas, reducing the degrees of freedom when extremes are studied in the frequency domain. Moreover, principal components are well correlated to the area-averaged thermal anomalies (third column) suggesting that a large portion of the EM is related to the interannual variability of the temperature itself.

The high correlations between F_a and T_a over the area defined from Figure 2 suggest a possible interesting interpretation of the nature of the temperature anomalies over these regions. A monthly temperature anomaly, in fact, can result either from the occurrence of extremely high anomalies lasting for a relatively short period, say few days, or from weaker anomalies persisting for a longer time. In the former case the temperature anomaly is associated with the occurrence of extreme events, whereas in the latter there is no relation between the anomaly and extremes. Therefore, the high correlation found between F_a and T_a indicates that, over the considered regions, the larger monthly temperature anomalies are generally associated with the occurrence of extremes.

3.2. Atmospheric and SST anomalies related to extreme months

Hereafter we describe the interannual variability of the extreme events and its link with the large scale circulation and SST, based on heterogeneous correlation maps. These maps are estimated by correlating the PC associated with the EM variability over a specific region (i.e., NW-EU, Med-EU, EU-Asia) with diverse atmospheric fields and SST. Differences related to extremes in T_{max} and T_{min}, as well as the intraseasonal variability of the patterns are also discussed.

3.2.1. NW-EU region

In agreement with the high correlations displayed in the left column of Table 1, a visual inspection of correlation maps confirms that atmospheric and SSTs anomalies connected with frequent extremes in T_{max} and in T_{min} over the NW-EU are similar. Therefore, for the sake of brevity, here we discuss only the results obtained from T_{max}. The analysis performed for T_{min} produces very similar results.

June. Correlation maps between extreme June conditions over NW-EU and a number of atmospheric parameters are presented in Figure 3. Anomalies in SKT (Fig. 3a) displays an area of positive correlations over NW-EU centred in the North Sea. Positive (negative) SST anomalies are found in the central-west North Atlantic (SE of Greenland), while a dipolar structure dominates the variability in the Mediterranean region, with positive (negative) correlations in the west-Mediterranean (Balcans). The correlations with the thermal field are particularly strong in the lower troposphere, with coherent correlations discernible in low-level thickness (Fig. 3c) and significant positive (negative) correlations in NW-EU (over Greece, western Turkey and Siberia). Barotropic anticyclonic anomalies dominate over NW-EU (Fig. 3b and 3d), with significant wind anomalies at low and high levels, and significant negative anomalies in precipitation (Fig. 3e). A belt of cyclonic anomalies extends (SW-NE) from the coast of Morocco up to the south-eastern Europe, covering the entire Mediterranean basin and then extending into central Russia. Moreover, there are significant SLP anomalies in the Artic region, increasing the meridional gradients in the northern portion of the Scandinavian Peninsula and contributing to low-level anomalous cold advections over north-central Russia (Fig. 3d). An extended view of the circulation anomalies associated with the extremes in NW-EU (Fig. 3f) shows a potential pattern of wave propagation from the blocking area into Asia.

July. While the summer marches on, the correlations related to extremes in NW-EU intensify (Figure 4). This feature found in both the thermal and the circulation fields. The blocking signature extend south-eastward while intensifying, having the local action centre over north Germany. Southward of the blocking system, high-level cyclonic anomalies dominate over the Mediterranean region, NW-Africa and the tropical North Atlantic with strong high-level wind anomalies encircling a cyclonic vortex over the eastern Mediterranean (Fig. 4b). At sea level, the low pressure still dominates the Artic region and significant anomalies extend over the North Atlantic (Fig. 4d). The blocking is associated with a local warm and dry troposphere, while cold and wet anomalies take

place over the eastern Mediterranean (Fig. 4a, 4c, 4e). The pattern of streamfunction anomalies (Fig. 4b) suggests a wave-train propagating from the eastern coast of North America to Europe, imprinting the skin temperature field. Interestingly, the wave-train seems to be better organized in correlation maps obtained for the extremes in T_{min} (Fig. 4f), where the remarkable wedge centred on the Greenwich meridian contributes to develop positive SSTs anomalies in the west Mediterranean basin (not shown) notably larger than those resulting from the T_{max} case (Fig. 4a).

August. Remarkable differences become evident comparing the anomalies related to extreme events during the early summer with those occurring in August (Figure 5). The blocking is now located at 60°N over Norway and the Norwegian Sea. A strong dipolar structure appears at 40°N, having the negative (positive) node over the Mediterranean basin, SE-Europe and Middle-East (eastward of the Caspian Sea) with the strongest correlations at higher levels (Fig. 5b). Signatures of that pattern are visible in the thermal field (also in the high level thickness; Fig. 5a, 5c) while significant deficit (surplus) of precipitation is observed over the blocking region and in the neighbourhoods of the Caspian and Aral Seas (the Mediterranean basin and south-eastern Europe; Fig. 5e). At sea level, negative pressure anomalies are still persistent at high latitudes, giving significant westerlies anomalies and probably affecting the intensity and location of the storm tracks (Fig. 5d). There are evidences of a wave-train propagating from the Great Lakes region through SW-Greenland to NW-EU (Fig. 5f) with imprints in the skin temperature field. This pattern of variability emerges in years during which the extratropical circulation is particularly perturbed.

3.2.2. Med-EU region

The visual inspection of the anomalies associated with extreme events over Med-EU confirms the high (low) level of correlation between extremes in T_{max} and T_{min} during June and August (July; Table 1, mid-column). Hereafter, we show results as obtained from the T_{max} analysis and we discuss the main differences between the anomalous climatology related to extremes in T_{max} and T_{min} in July. In the early summer extremes are associated with barotropic patterns, while in July and August, baroclinic structures became dominant.

June. Frequent extremes in Med-EU in the early summer (Figure 6) are linked with anomalous warming of the Mediterranean SSTs and positive SKT anomalies over central Europe and NW-Africa, while coastal Atlantic SSTs remain almost unperturbed (Fig. 6a). The anomalous warming is observed at all tropospheric levels (but larger correlations are at lower levels; Fig. 6c) and it is associated with barotropic positive anomalies in circulation (Fig. 6b). A belt of cyclonic anomalies

zigzags through the high latitudes, from SE Greenland to Eurasia, intensifying gradients and enhancing advections (Fig. 6d). Another dominant cyclonic anomaly centre is located over NW-Africa. In skin temperature there is also a remarkable cold area in the neighbourhood of the Caspian and Aral Seas, where correlations with the OLR suggest that anomalous cloudy skies could be playing a role when filtering the downward short wave radiation (not shown).

July. As suggested by the low correlation in Table 1 and illustrated in Figure 7, extreme events in T_{max} and T_{min} are connected with somewhat diverse climatic anomalies. The main difference concerns the anomalous warming of the Mediterranean SSTs. When there are extremes in T_{min} the anomalous warming is even more extended: it peaks in the Mediterranean Sea and extends over the full basin and over land coastal points of North Africa and Eastern Europe (Fig. 7a). On the other hand, extremes in T_{max} occur when there is anomalous warming over the western part of the basin and over a large portion of the European continent (Fig. 7d). In the T_{max} case, significant cyclonic SLP anomalies are confined in the neighbourhoods of the Iberian Peninsula (Fig. 7c). On the contrary, when extremes are in T_{min} cyclonic anomalies also extends over north-east Africa, advecting warm air from the Sinai into the eastern Mediterranean sector (Fig. 7f). There are also noticeable differences in the high-level circulation (Fig. 7b, 7e). Extremes in T_{min} are associated with a dipolar structure with positive (negative) nodes centred in the neighbourhoods of Italy (Caspian Sea). The local correlations with the thickness are larger in the T_{max} than in the T_{min} case, but for the T_{min} extremes, atmospheric correlations almost vanish at high-levels (not shown).

August. The main characteristic of the anomaly circulation associated with extremes over Med-EU in August is the lack of significant barotropic structures (Fig. 8b, 8d). At low levels there are generalized cyclonic anomalies (Fig. 8d), with significant anomalous convergence in the subtropical Northwest Africa, suggesting anomalies in the African monsoon (correlations in precipitation denote the northward displacement of the convective systems; not shown). The surface warming maximizes over the central Mediterranean, but large positive SKT anomalies affect also the central Europe, Balkans and Mediterranean coastal lands in Turkey, Middle-East, North Africa and Morocco (Fig. 8a). The anomalous heating is also visible in thickness anomalies (Fig. 8c, 8e). The amplitude of the positive node in thickness correlations diminishes with increasing height while the structure of the pattern becomes similar to that in high-level circulation. A notable feature displayed in Fig. 8f-8g is the baroclinic sea-saw that dominates the variability in the subtropical region, with opposite nodes in the Pacific and Atlantic sectors (positive streamfunction anomalies in the southern hemisphere are cyclonic anomalies).

3.2.3. EU-Asia

Extreme events in EU-Asia are associated with anomalous blocking patterns. The intensity of the correlations and the related systems are remarkably modulated by intraseasonal variability.

June. During the early summer (Figure 9), the blocking signature is particularly strong. Positive anomalies in eddy streamfunction (Fig. 9b) are centred over NW-Russia with significant high-level wind anomalies, subsidence (Om500 is not shown), negative anomalies in precipitation (not shown) and divergence at surface levels (Fig. 9d). The thermal field denotes positive anomalies in skin temperature (Fig. 9a) and low-level thickness (Fig. 9c), and a zonally elongated pattern of positive high-level thickness anomalies that connects the continental anomalies with those upstream of the blocking, associated with northward displacement of the Azores anticyclone. Downstream of the blocking, there is an extended area of cyclonic anomalies with a strong action centre over central Russia (anomalies are also visible in skin temperature and low-level thickness). This system seems to be part of a wave train of anomalies propagating as far as eastern Siberia (Fig. 9e, 9f).

July. One month later, the blocking related correlations diminish while the blocking action centre moves southward (Fig. 10b). The local warming is also visible in thickness anomalies (Fig. 10a, 10c). Cyclonic anomalies encircle the blocking structure at low levels (fig. 10f), and significant negative correlations in SLP covers large portion of Europe, Mediterranean Sea and North Africa (Fig. 10d). At high levels there is a strong circulation gradient downstream of the blocking anomalies, with alternant signs and barotropic structure, which resembles a wave train propagating into Southeast-Asia (Fig. 10e, 10f).

August. By the end of the summer (Figure 11), the anomalous climatology related to extremes in EU-Asia seems to be organized in a wave pattern with positive (negative) circulation anomalies affecting the Azores anticyclone (Iceland low) up to reaching the blocking sector (Fig. 11b, 11d). While anomalies in skin temperature and low-level thickness are non-significant in the central North Atlantic, the other two nodes are significant (Fig. 11a, 11c). Imprints of those nodes are also visible in precipitation anomalies (not shown). Downstream of the blocking, the perturbation affects also the Middle-East and central Asia (Fig. 11e). Extended cyclonic anomaly affecting the Middle-East and SE-Asia does not give significant anomalies in OLR (in concordance with non-significant anomalies in both precipitable water and upward winds; not shown).

3.3. Stability of the patterns

In order to check the robustness of the results described in Section 3.2, the same methodology is now applied to monthly indexes of extremes defined by imposing a more restrictive threshold. Specifically, we repeat the analysis using the percentile 90 (P90) as threshold in the definition of extreme days instead of the percentile 75 (P75). Therefore, now the EM series are based on extremes at P90 and will be named EM90. The sensitivity of the extreme events classification to the imposed threshold is analyzed by comparing both the leading loadings that define the European sub-domains and the large scale conditions associated with frequent extremes over those regions.

In order to verify that the EOF analysis applied to the P75 and P90 data sets produces similar results we have compared the loadings and computed the correlations between the principal components obtained for the two cases. In general, the correlations are high (see Table 3) and the loadings similar (not shown), especially for the NW-EU and EU-Asia regions. Consistent with these findings, the anomalies in the large scale circulation discussed in Section 3.2 for the P75 case are similar to those obtained for the P90 case (not shown). In conclusion, the change from the P75 threshold to a more restrictive one (P90) does not alter the main results of our analysis.

4. Analysis of the European 2003 heatwave

After having described the large scale anomalies related to European heatwaves, we want to tackle the issue as to whether our method is able to capture the signature of the record-breaking 2003 event. Hereafter we present some results obtained when our method is applied to the full time series covering the period 1958-2004 (i.e., including 2003). In particular, descriptions are focused on June and August, since results for July do not substantially differs from those obtained for June.

4.1. Reconstruction of the European 2003 heatwave

Top panels in Figure 12 present the EM index for June and August 2003 (i.e., the number of extreme days registered in June/August 2003), while bottom panels display their reconstruction based on the linear combination of the first 5 un-rotated components obtained from the EOF analysis applied to the entire 1958-2004 period (i.e., including 2003). The 2003 heatwave in June (Fig. 12a) presents action centres over the Euro-Mediterranean region and the North-West Europe. There are not remarkable differences when the heatwave is defined through extremes in T_{max} or in T_{min} (not shown). The transition from June to July is characterized by more frequent extremes in the Mediterranean Sea (not shown). Although we have strongly reduced the degrees of freedom of the system (the reconstruction based on the first 5 leading modes explains about the 65% of the total variance), the leading un-rotated modes are able to capture the imprints of the observed heatwave in June (Fig. 12b) and July (not shown). The best fit is obtained over the Euro-Mediterranean region while the magnitude of anomaly over North-West Europe is slightly underestimated. In the following sub-section, we will illustrate the case of June-2003 in T_{max}.

Figure 12e presents the long-term area-averaged anomalies of T_{min} and T_{max} over France, for August. The figure illustrates how the T_{min} anomaly has broken the record in August of 2003 peaking at 5 standard deviations. On the other hand, the anomaly in T_{max} has only reached 1.5 standard deviations and other years have registered even larger anomalies. Furthermore, the frequency of extreme days registered in T_{min} during August of 2003 was also notably greater than that in T_{max} (not shown). For this reason, the August 2003 heatwave will be discussed in terms of extremes in T_{min}. The potential mechanism for elevating the T_{min} in August 2003 has been discussed by Black et al. (2004).

The signal of August 2003 heatwave in T_{min} is notably strong (Fig. 12c), with more than 24 days (out of 31) with minimum temperature above the 75th percentile over most of central Europe (and exceeding the 90th percentile over large part of the domain southward of 50°N; not shown). The reconstructed map (Fig. 12d) captures the spatial pattern of the heatwave well and gives a good indication about its intensity, with a large number of extreme days over the Euro-Mediterranean while the frequence of the extreme days diminishes in the northern sector of the domain and over the Eurasia.

4.2. Atmospheric and SST anomalies related to a 2003-like heatwave

In this section, we concentrate the attention on those EOF loading patterns with a PC which peaks in 2003. The leading modes associated with June and August 2003 extreme variability locally maximize over NW-EU and Med-EU. Table 4 illustrates the agreement between the temporal variability of those modes and the analogous modes discussed in Section 3, when the EOF was applied to EM series in which the year 2003 was removed. A remarkable difference between the previous results and the 2003 case regards both the amplitude and the persistence of the extremes, especially in August of 2003. The mode that dominates the August 2003 heatwave in T_{min} explains the 36% of the total variance and its PC peaks in 2003 exceeding 4.6 standard deviations. It could be certainly considered an "outlier".

Hereafter, we present composite maps in which "2003-like" anomalies were clustered. Selected years are those in which the PCs exceed one standard deviation, and peaks in the positive phase according to the anomaly registered in 2003. The 2003-like composite maps capture some large-scale anomalies as those described in previous papers when analyzing the 2003 heatwave, and "others" that compete to favour extremes in particular regions.

4.2.1 June 2003-like composites

There are 5 cases contributing to the composite anomalies describing a June 2003-like extreme month over Med-EU (1964, 1981, 2000, 2002 and 2003; Figure 13 left column). Extreme conditions are associated with large SKT anomalies over Europe and the Mediterranean Sea. As described by Black et al. (2004), there is a pattern with altering positive and negative banded SST anomalies in the North Atlantic, although statistical significance is only reached in the cold pool SE of Greenland. Circulation anomalies are also consistent with those illustrated by e.g., Black et al. (2004) and Cassou et al. (2005): anticyclonic anomalies extend from the central-west North Atlantic

to Europe and cyclonic anomalies at extratropical latitudes, with a node located SE of Greenland. This pattern shows a southward shift of the Icelandic low and a consequent shift of the stormtracks. Previous studies have discussed about anomalies in the African monsoon during June 2003 (e.g., Black et al. 2004, Cassou et al. 2005). Our composite displays enhanced convection over the tropical North Africa and negative precipitation anomalies over Europe (not shown), though these anomalies appear to be barely significant when a 95% significance level is considered. One-month lagged composite anomalies in SKT (Fig. 13d) illustrate how the anomalous warming in the Mediterranean SST has dominated the regional anomalous climatology in May, an anomaly that is not found in the two-month lagged plots (not shown). This result is in agreement with the strong warming of the Mediterranean Sea registered from April to May of 2003 (e.g., Black et al. 2004, Grazzini and Viterbo 2003).

An anomalous composite over NW-EU is made using 7 years (1960, 1966, 1970, 1976, 1989, 1992 and 2003; Figure 13, right column). Extreme events in NW-EU are related to anomalous warm temperatures over a region centred in the North and Norwegian Seas, United Kingdom and Scandinavian Peninsula. The SST anomalies extend southward, displaying a warm tongue off the Portugal and Morocco coasts similar to the result found for June 2003 (Black et al., 2004), though in this case the amplitude of the anomaly is not statistically significant. The 2003-like composites for NW-EU present Nina-like anomalies in the tropical Pacific sector similar to the results found for the Med-EU case (figures not shown). Composites also display anomalous blocking conditions over NW-EU and non-significant negative anomalies in SLP over NW Africa (Fig. 13f).

4.2.2 August 2003-like composites

Composites of anomalies in the Mediterranean sector have the strong imprint of the 2003 year. There are only 3 years in this composite (1962, 1966 and 2003; Figure 14, left column): the PC in 2003 peaks at 4.6 standard deviations while in 1962 (1966) it peaks at 1 (1.2) standard deviations. Therefore, it appears rather evident that August 2003 has quite unique characteristics, as also noted by e.g., Schär et al. (2004). The main feature of the anomaly patterns obtained from composites is their regional nature. SKT anomalies are positive in the Mediterranean Sea, southern Europe and the northern portion of Africa (with a reversal sign of anomalies southward of 15°N). High-level circulation is characterized by anticyclonic anomalies, without discernible wave propagations, suggesting that August 2003-like years are the result of local interactions. The mass field anomalies have a baroclinic character, displaying significant cyclonic anomalies over North Africa probably related to local anomalies in the Hadley cell. Previous studies have described August 2003 as a

month characterized by above (below) average precipitation over the Sahel (along the Guinea coast), resulting from the northward migration of the African monsoon (Cassou et al. 2005). Unfortunately, due to the limitation of the global observational dataset, we can not show and discuss the composites of either OLR and precipitation for this case.

5. Discussion

In this paper we present a methodology to detect extreme climatic conditions over Europe and to identify the anomalies in the large scale circulation associated with these extremes. In order to test the ability of our approach to capture the extremes and the associated large scale anomalies, we showed and discussed, in some detail, the summer 2003 heatwave as a case study. From the results shown in Section 4, our methodology appears to be able to detect the main features of the event, especially for the month of June. Furthermore, the characteristics of the large scale anomalies associated with the 2003 heatwave are fully consistent with the results found in previous studies (e.g., Black et al. 2004, Cassou et al. 2005).

More generally, the results we obtained from the analysis of the extremes in surface temperature over Europe show well defined anomaly patterns in the general circulation and SSTs. Extreme events over the north-west Europe and over Eurasia are typically related to blocking anomalies. The intraseasonal variability of those patterns is related with the amplitude of the correlations, the relative location of the action centers and the wavetrains downstream or upstream of the extremes centre. On the other hand, extremes over the Euro-Mediterranean region are associated with weak blockings in June and with baroclinic pattern of anomalies in July and August, probably related with the regional shifts of the descending branch of the Hadley circulation. Extremes over the Euro-Mediterranean region in July are also linked with the anomalous warming of the Mediterranean SSTs.

We also notice that large scale circulation anomalies associated with extreme events sometimes resemble the patterns of interannual variability found in other works. For example, the Mediterranean dipole in our Figures 3 and 4 resembles the anti-phase anomalies described by Corte-Real et al. (1995) which they have attributed to blocking situations over the North Atlantic accompanied by depressions in the Mediterranean sector. A similar picture is also in Figures 5 and 6 by Xoplaki et al. (2003b; hereafter X03b) were the east-west dipole in the Mediterranean summertime temperature anomalies is described as associated with a jet stream meandering between cyclonic and anticyclonic anomalies extending from SE Greenland to the Caspian Sea. It is interesting that different approaches recover similar patterns. If we refer to extreme events in the Mediterranean region, the patterns in our Figure 6 appear like those in Figure 3 by X03b when describing warm conditions over the central Mediterranean associated with local anomalous blocking conditions, subsidence and stability.

Interestingly our patterns present a number of similarities with results from X03b, although we apply a completely different approach. The main difference is that X03b studied summertime temperature series, while we consider only temperatures exceeding thresholds, in order to focus on the variability of extreme cases in the frequency domain. Therefore, the data considered in the two studies contain different kind of information and our approach is based on the variability of the portion of spectrum related to the extreme cases. Moreover, in our analysis we have generalized the results over diverse European sub-domains and included the intraseasonal variability.

Furthermore, the similarities between the large-scale anomaly patterns associated with extremes we have found and the patterns of interannual climate variability found in other studies raise the important question as to whether the patterns of interannual variability are biased by the occurrence of extremes. Special attention must be devoted in exploring how much the modes related to the variability of extreme events are different from those explaining the “no-extreme variability” or, in other words, are extremes occurring as a result of a peak in the activity of some particular climate variability mode? To address this point, we have repeated our analysis using time series in which the extremes from the upper and lower tail of the statistical distribution have been removed (no-extreme cases are when temperature is falling in the interval P25 to P75). In this case, the variability spreads into a large number of modes each of one explains few percentage of variance. Modes explaining the variability of the extreme events are also present in the no-extreme case suggesting that extreme events occur when some mode of the “no-extreme variability” strongly peaks. This result seems to suggest that extreme climatic events, as defined in our approach, may occur as a strong peak of a mode of climate variability.

6. Conclusions

Although the society in general is vulnerable to the increasing extreme events (Kunkel et al., 1999), Southern Europe is expected to find itself in a situation particularly compromising in a near future, threat from both heatwaves and the reduction of water resources (IPCC 2001). The level of knowledge regarding both the local-interactions and the anomalous climatic conditions in which extremes are embedded is the first constraint for their seasonal prediction, as well as for preparing our society to mitigate the effects of those more severe and frequent extremes that are expected to occur in a warmer climate (e.g., Klein Tank and Können 2003).

Whereas in a classical framework the study of heatwaves is done by analyzing singular weather systems that favors local anomalies, weather and climate are sometimes overlapping concepts. There are some years during which those weather systems are more frequent and the successive occurrence of heatwaves is perceived as an extremely anomalous month, with disastrous consequences for humans, ecosystems and lands that are critically stressed without having the necessary time to recover. This paper describes the large scale circulation associated with those extreme months signed by the imprints of heatwaves.

The methodology to detect extreme climatic conditions and to classify heatwaves over Europe is based on empirical orthogonal functions applied to monthly indexes of extremes, defined as the frequency of days with temperatures crossing thresholds. We have identified three regions of relevance to study extreme events over Europe: the north-west Europe, the Euro-Mediterranean region and Eurasia. Extremes over those regions are related with well defined anomalous patterns in both atmospheric circulation and SSTs.

Extreme events over the north-west Europe are typically related to blockings. Anomalous barotropic structures are particularly strong (weak) in July (June), when anomalies seems to be organized in a wavetrain patterns that propagates from USA to NW-EU (from the blocking region into Asia). In agreement with results by other authors (Xoplaki et al. 2003a, Xoplaki et al. 2003b, Corte Real et al. 1995), we also find an opposite relation between the pattern of anomalies in the blocking region and over the eastern Mediterranean. Blocking anomalies in August disrupt a particularly perturbed extratropical circulation. The blocking is the counterpart of a dipolar structure that dominates the anomalous variability over Europe with the negative barotropic node over the Euro-Mediterranean sector.

In June, anomalous climate conditions associated with extremes over the Euro-Mediterranean region are weak blocking situations. In July and August baroclinic patterns of anomalies dominate the variability related to the occurrence of extreme events over that region. In a blocking condition, the physical processes that might produce local intense heating anomalies are the surplus of short wave radiation reaching the surface and the vertical motion favoring the adiabatic warming. Baroclinic anomalies, on the other hand, might be related to regional changes (shifts) of the descending branch of the Hadley circulation.

Another important region in terms of occurrence of extreme surface temperature is Eurasia. Also in this case, blocking anomalies dominate the extreme events variability. The large scale anomalies for June mainly differs from that for July in the intensity of the patterns (their amplitude diminishes in July) and in the location of the main cyclonic node, downstream of the blocking. In June (July) a wave train appears to propagate from the blocking pattern into North (South) Asia. Blockings in August appears as the last node in a wave train propagating from the central-west North Atlantic to EU-Asia.

Large scale circulation anomalies associated with extreme events sometimes resemble the patterns of interannual variability found in previous works. We suggest that modes explaining the variability of the extreme events are intrinsic modes of the “normal” variability and extremes occur when some mode strongly peaks. On other words, we suggest that extreme climatic events, as defined in our approach, may occur as a strong peak of a mode of climate variability.

As a next step, our method will be applied to a set of model integrations conducted using the INGV-SXG CGCM (Gualdi et al. 2006). The first goal is to assess the capability of the model to reproduce the characteristics of the extreme climate variability. Then, a second objective is to explore the extent to which those characteristics, as well as the associated anomalies, could potentially be predicted with a seasonal leading time. Finally, possible changes under particular climate change scenarios will also be investigated.

Acknowledgments. First author was partially supported by MERSEA (SIP3-CT-2003-502885) and ENSEMBLES (GOCE-CT-2003-505539) European funding projects.

7. References

Beniston M., 2004: The 2003 heatwave in Europe: A shape of things to come? An analysis based on Swiss climatological data and model simulations. Geophys. Res. Lett. 31: L02202, doi:10.1029/2003GL018857.

Beniston M, H.F. Diaz, 2004: The 2003 heat wave as an example of summers in a greenhouse climate? Observations and climate model simulations for Basel, Switzerland. Global and Planetary Change, 44, 73-81.

Beniston M., D. B. Stephenson, 2004: Extreme climatic events and their evolution under changing climatic conditions. Global and Planetary Change, 44, 1-9.

Black E., M. Blackburn, R.G. Harrison, B.J. Hoskins, B.J. and J. Methven, 2004: Factors contributing to the summer 2003 European heatwave Weather, 59, 8, 217-223, doi:10.1256/wea.74.04

Bolle H.-J., 2002: Climate, climate variability and impacts in the Mediterranean area: An overview. Chapter 2 in Mediterranean Climate, H.-J. Bolle Editor, Springer.

Cassou C., L. Terray and A.S. Phillips, 2005: Tropical Atlantic forcing and predictability of extreme warm events in Europe. J. Climate Letter, 18, 2805-2811.

Cattell R.B., 1966: The scree test for number of factors. Multivariate Behavioral Res., 1, 245-276.

Corte-Real J., X. Zhang and X. Wang, 1995: Large-scale circulation regimens and surface climatic anomalies over the Mediterranean. Int. J. of Climatology, 15, 1135-1150.

Della-Marta P.M., J Luterbacher, H. von Weissenflush, E. Xoplaki, M. Brunet and H. Wanner, 2007: Summer heat waves over western Europe 1880-2003, their relationship to large scale forcings and predictability. Clim. Dyn., In press.

Easterling, D.R., J.L. Evans, P.Ya. Groisman, T.R. Karl, K.E. Kunkel and P. Ambenje, 2000: Observed variability and trends in extreme climate events: A brief review. Bull. Am. Meteorol. Soc., 81, 417-425.

Fink, A.H., T Brücher, a. Krüger, G.C. Leckebusch, J.G. Pinto and U. Ulbrich, 2004: The 2003 European summer heatwaves and drought – synoptic diagnosis and impacts. Weather, 59 (8), 209-216.

Giogi F., 2002: Variability and trends of sub-continental scale surface climate in the twentieth century. Part I: Observations. Clim. Dyn., 18: 675-691.

Grazzini F. and P. Viterbo, 2003: Record-breaking warm sea surface temperature of the Mediterranean Sea. ECMWF Newsletter, 98, 30-31.

Gualdi S., E. Scoccimarro and A. Navarra, 2006: Changes in Tropical Cyclone Activity due to Global Warming: Results from a High-Resolution Coupled General Circulation Model. J. of Clim., submitted.

Haylock M.R. and C.M. Goodess, 2004: Interannual variability of European winter rainfall and links with mean large-scale circulation. Int. J. of Climatol., 24, 759-776.

IPCC, 2001: Climate Change. The IPCC Third Assessment Report. Volumes I (Science), II (Impacts and Adaptation) and III (Mitigation Strategies). Cambridge University Press, Cambridge.

Jones, P.D. and A. Moberg, 2003: Hemispheric and large-scale surface air temperature variations: An extensive revision and an update to 2001. J. Climate, 16, 206-223.

Kalnay E. and Coauthors, 1996: The NCEP/NCAR 40-year Reanalysis Project. Bull. Amer. Meteorol. Soc., 77, 437-471.

Kistler E. and Coauthors, 2001: The NCEP/NCAR 50-Year Reanalysis: monthly means CD-ROM and documentation. Bull. Am. Met. Soc., 82: 247-267

Klein Tank, A. M. G. and Coauthors, 2002: Daily dataset of 20th century surface air temperature and precipitation series for the European Climate Assessment. Int. J. Climatol., 22, 1441-1453.

Klein Tank A.M.G. and G.P. Können, 2003: Trends in Indices of daily temperature and precipitation extremes in Europe, 1946-99. J. Climate, 16, 3665-3680.

Kunkel, K.E., R.A. Pielke and S.A. Changnon, 1999: Temporal fluctuations in weather and climate extremes that cause economic and human health impacts: a review. Bull. Am. Meteorol. Soc. 80, 1077-1098.

Liebmann B. and C. A. Smith, 1996: Description of a Complete (Interpolated) Outgoing Longwave Radiation Data Set. Bull. Am. Met. Soc., 77, 1275-1277.

Luterbacher J., D. Dietrich, E. Xoplaki, M. Grosjean and H. Wanner, 2004: European seasonal and annual temperature variability, trends and extremes since 1500 A.D., Science, 303, 1499-1503. DOI 10.1126/science.1093877.

Nakamura M., T. Enomoto and S. Yamane, 2005: A simulation study of the 2003 heatwave in Europe. J. of the Earth Simulator, 2, 55-69.

Ogi M., K. Yamazaki and Y. Tacibana, 2005: The summer northern annular mode and abnormal summer weather in 2003. Geophys. Res. Lett. 32, L04706, doi:10.1029/2004GL021528.

Richman M.B., 1986: Review article: Rotation of principal components. Int. J. Climatol., 6, 293-335.

Schär C., P.L. Vidale, D. Lüthi, C. Frei, C. Häerli, M.A. Linie and C. Appenzeler, 2004: The role of increasing temperature variability in European summer heatwaves. Nature, 427, 332-336.

Spiegel M.R. and L.J. Stephens, 1961: Theory and problems of statistics. Schaum's outlines of, McGraw Hill.

Stott P.A., D.A. Stone and M.R. Allen, 2004: Human contribution to the European heatwave of 2003, Nature, 432, 610-614, doi:10.1038/nature03089

Trigo R. M., R. Garcia-Herrera, J. Diaz, I. F. Trigo and M.A. Valente, 2005: How exceptional was the early August 2003 heatwave in France? Geophys. Res. Lett., 32, L10701, doi:10.1029/2005GL022410

Yan Z., P.D. Jones, T.D. Davies, A. Moberg, H. Bergstrom, D. Camuffo, C. Cocheo, M. Maugeri, G.R. Demaree, T. Verhoeve, E. Thoen, M. Barriendos, R. Rodriguez, J. Martin-Vide and C. Yang, 2002: Trends of Extreme Temperatures in Europe and China based on Daily observations. Climatic Change, 53, 355-392

Xie P. and P.A. Arkin, 1997: Global precipitation: a 17-year monthly analysis based on gauge observations, satellites estimates and numerical model outputs. Bull. Am. Met. Soc., 78, 2539-2558.

Xoplaki E., J.F. Gonzalez-Rouco, D. Gylistras, J Luterbacher, R. Rickli and H. Wanner, 2003a: Interannual summer air temperature variability over Greece and its connection to the large-scale atmospheric circulation and Mediterranean SSTs 1950-1999. Clim. Dyn. 20: 537-554.

Xoplaki E., J.F. Gonzalez-Rouco, J Luterbacher and H. Wanner, 2003b: Mediterranean summer air temperature variability and its connection to the large-scale atmospheric circulation and SSTs. Clim. Dyn. 20: 723-739.

Tables

a) June, PCs correlation T_{max} **vs.** T_{min} **extreme areas**	**NW-EU (T_{min}, 12%)**	**Med-EU (T_{min}, 11%)**	**EU-Asia (T_{min}, 16%)**
NW-EU (T_{max}, 14%)	0.77		
Med-EU (T_{max}, 13%)		0.71	
EU-Asia (T_{max}, 18%)			0.67
b) July, PCs correlation T_{max} **vs.** T_{min} **extreme areas**	**NW-EU (T_{min}, 20%)**	**Med-EU (T_{min}, 12%)**	**EU-Asia (T_{min}, 16%)**
NW-EU (T_{max}, 21%)	0.84		
Med-EU (T_{max}, 9%)		0.47	
EU-Asia (T_{max}, 16%)			0.70
c) August, PCs correlation T_{max} **vs.** T_{min} **extreme areas**	**NW-EU (T_{min}, 23%)**	**Med-EU (T_{min}, 14%)**	**EU-Asia (T_{min}, 8%)**
NW-EU (T_{max}, 28%)	0.94		
Med-EU (T_{max}, 13%)		0.90	
EU-Asia (T_{max}, 12%)			0.76

Table 1*: Principal components (PCs) from extremes in T_{max} correlated against PCs from extremes in T_{min}. The correlations are calculated for every area related to frequent extremes. Panel a) is for June, b) for July and c) for August. The explained variance of the loadings determining every area is indicated between brackets. All the correlations are statistically significant at 99.5%*

a) June, T_{max} analysis				d) June, T_{min} analysis			
Region	**PC-F_a**	**PC-T_a**	**F_a-T_a**	**Region**	**PC-F_a**	**PC-T_a**	**F_a-T_a**
NW-EU	0.86	0.85	0.98	**NW-EU**	0.97	0.95	0.98
Med-EU	0.94	0.92	0.97	**Med-EU**	0.94	0.91	0.96
EU-Asia	0.98	0.95	0.97	**EU-Asia**	0.98	0.94	0.97
b) July, T_{max} analysis				**e) July, T_{min} analysis**			
Region	**PC-F_a**	**PC-T_a**	**F_a-T_a**	**Region**	**PC-F_a**	**PC-T_a**	**F_a-T_a**
NW-EU	0.97	0.95	0.98	**NW-EU**	0.96	0.95	0.98
Med-EU	0.93	0.88	0.95	**Med-EU**	0.94	0.91	0.98
EU-Asia	0.92	0.87	0.95	**EU-Asia**	0.95	0.93	0.98
c) August, T_{max} analysis				**f) August, T_{min} analysis**			
Region	**PC-F_a**	**PC-T_a**	**F_a-T_a**	**Region**	**PC-F_a**	**PC-T_a**	**F_a-T_a**
NW-EU	0.95	0.93	0.98	**NW-EU**	0.98	0.96	0.97
Med-EU	0.94	0.92	0.98	**Med-EU**	0.97	0.95	0.98
EU-Asia	0.95	0.93	0.98	**EU-Asia**	0.87	0.83	0.97

***Table 2**: Correlations among PCs and area-averaged indexes; F_a is the anomaly of extreme temperature frequency area-averaged and T_a is the area-averaged temperature anomaly time series. Left (right) panels present correlations related to extremes in T_{max} (T_{min}). Correlations are for June (a-d), July (b-e) and August (c-f). All the correlations are statistically significant at 99.5%*

a) June, T_{max} analysis				d) June, T_{min} analysis			
P75 vs P90	**NW-EU**	**Med-EU**	**EU-Asia**	**P75 vs P90**	**NW-EU**	**Med-EU**	**EU-Asia**
NW-EU	0.96			**NW-EU**	0.86		
Med-EU		0.74		**Med-EU**		0.93	
EU-Asia			0.93	**EU-Asia**			0.94
b) July, T_{max} analysis				**e) July, T_{min} analysis**			
P75 vs P90	**NW-EU**	**Med-EU**	**EU-Asia**	**P75 vs P90**	**NW-EU**	**Med-EU**	**EU-Asia**
NW-EU	0.96			**NW-EU**	0.86		
Med-EU		**0.58**		**Med-EU**		**0.58**	
EU-Asia			0.97	**EU-Asia**			0.90
c) August, T_{max} analysis				**f) August, T_{min} analysis**			
P75 vs P90	**NW-EU**	**Med-EU**	**EU-Asia**	**P75 vs P90**	**NW-EU**	**Med-EU**	**EU-Asia**
NW-EU	0.96			**NW-EU**	0.96		
Med-EU		0.74		**Med-EU**		0.96	
EU-Asia			0.97	**EU-Asia**			0.78

***Table 3**: PCs from extremes defined at percentile 75 correlated among PCs when extremes are defined at percentile 90. Left (right) panels present correlations related to extremes in T_{max} (T_{min}) analysis. Correlations are for June (a-d), July (b-e) and August (c-f). All the correlations are statistically significant at 99.5%*

a) June, T_{max} related correlations		
Removing 2003 vs. 2003-like case	**NW-EU (2003-like)**	**Med-EU (2003-like)**
NW-EU (Clim.)	0.99 (0.91)	
Med-EU (Clim.)		0.98 (0.92)
b) August, T_{min} related correlations		
Removing 2003 vs. 2003-like case	**NW-EU (2003-like)**	**Med-EU (2003-like)**
NW-EU (Clim.)	0.98 (0.96)	
Med-EU (Clim.)		0.79 (0.71)

***Table 4**: Correlations between the PC associated to the EOF loading patterns from the 1958-2004 (without 2003) analysis and those PCs associated to the EOF loading patterns from the 1959-2004 (with 2003; namely 2003-like) analysis, at P75 and at P90 (between brackets). Panel a) is for June when the extremes are in T_{max}. Panel b) is for August and refers to extremes in T_{min}. All the correlations are statistically significant at 99.5%*

Figure captions

Figure 1: Mean number of extreme days in T_{max} per month, during July. Units are days/month.

Figure 2: Rotated EOF loadings from EM series, displaying the areas of frequent extremes in T_{max}. Isolines are every 3 non-dimensional units, the zero isoline is removed and shading emphsizes the regions where the number of days per month with extremes temperatures has the largest variability. The leading structures denote regions of high variability over three European sub-domains: north-western Europe (NW-EU, left column), Euro-Mediterranean (Med-EU, middle column) and Eurasia (EU-Asia, right column). Top-row is for June, middle-row for July and bottom-row for August.

Figure 3: Correlation maps between the PC associated with the variability of extremes in T_{max} over the NW-EU in June, and diverse large-scale fields: a) skin temperature, b) high-level eddy streamfunction and winds at 200 hPa., c) low-level thickness, d) sea level pressure and surface winds e) precipitation and f) high-level eddy streamfunction (extended view). Contours are every 0.1 (but every 0.2 for the precipitation), the zero line is omitted and significant anomalies at the 95% confidence level are shaded. Correlation vectors with modulus lower than 0.5 are obscured.

Figure 4: Same as Fig. 3 (from a to e), but for July. In addition, f) is an extended view of correlations with high-level eddy streamfunction but for the T_{min} case.

Figure 5: Same as Fig. 3, but for August.

Figure 6: Correlation maps between the PC associated with the variability of extremes in T_{max} over the Med-EU in June, and diverse large-scale fields: a) skin temperature, b) high-level eddy streamfunction and winds at 200 hPa., c) low-level thickness and d) sea level pressure and surface winds. Contours are every 0.1, the zero line is omitted and significant anomalies at the 95% confidence level are shaded. Correlation vectors with modulus lower than 0.5 are obscured.

Figure 7: Correlation maps between the PC associated with the variability of extremes in T_{max} (left column) and in T_{min} (right column) over the Med-EU in July, and diverse large-scale fields: a-d) skin temperature, b-e) high-level eddy streamfunction and winds at 200 hPa. and c-f) sea level

pressure and surface winds. Contours are every 0.1, the zero line is omitted and significant anomalies at the 95% confidence level are shaded.

Figure 8: Correlation maps between the PC associated with the variability of extremes in T_{max} over the Med-EU in August, and diverse large-scale fields: a) skin temperature, b) high-level eddy streamfunction and winds at 200 hPa., c) low-level thickness, d) low-level eddy streamfunction e) high-level thickness, f) high-level eddy streamfunction (extended view) and g) low-level eddy streamfunction (extended view). Contours are every 0.1, the zero line is omitted and significant anomalies at the 95% confidence level are shaded. Correlation vectors with modulus lower than 0.5 are obscured.

Figure 9: Correlation maps between the PC associated with the variability of extremes in T_{max} over the EU-Asia in June, and diverse large-scale fields: a) skin temperature, b) high-level eddy streamfunction and winds at 200 hPa., c) low-level thickness, d) sea level pressure and surface winds,e) high-level eddy streamfunction (extended view) and f) low-level thickness (extended view). Contours are every 0.1, the zero line is omitted and significant anomalies at the 95% confidence level are shaded. Correlation vectors with modulus lower than 0.5 are obscured.

Figure 10: Same as Fig. 9, but for July.

Figure 11: Same as Fig. 9 (a-e), but for August.

Figure 12: a, c) Total number of days during which the daily maximum (minimum) temperature in June (August) of 2003 is in the fourth quartile; b, d) the reconstruction of the observed frequency of extremes using the five leading EOFs; and e) time series displaying the observed box-averaged anomalies of T_{max} (red) and T_{min} (blue) in August, as a function of the years. Box in which anomalies were averaged is over France (0°-7.5°E, 42.5°N-50°N) and anomalies are expressed in standard deviations.

Figure 13: Anomaly composites related to frequent extremes in T_{max} over the Med-EU (left column) and NW-EU (right column) in June 2003-like years: a-e) skin temperature, b-f) sea level pressure, c-g) high-level eddy streamfunction, d) one month lagged skin temperature. Anomalies are expressed in standard deviations. Contours are every 0.2, the zero line is omitted and significant anomalies at the 95% confidence level are shaded.

Figure 14: Anomaly composites related to frequent extremes in T_{min} over the Mediterranean sector in August 2003-like years: a) area where the frequency of the extremes maximize, b) skin temperature, c) sea level pressure, d) high-level eddy streamfunction. Anomalies are expressed in standard deviations. Contours are every 0.3, the zero line is omitted and significant anomalies at the 95% confidence level are shaded.

Figure 1, Carril et al., 2007
Mean frequence of observed extremes in Tmax, July

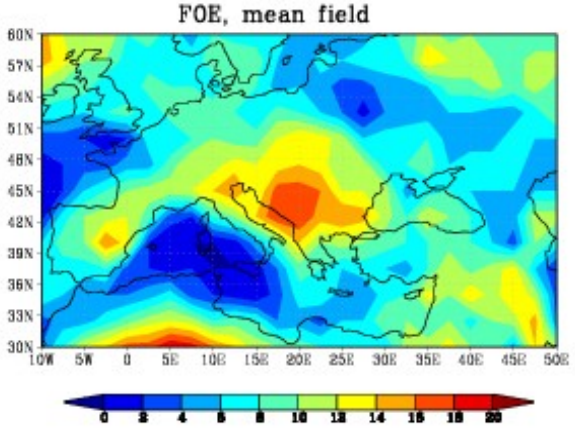

Figure 2, Carril et al., 2007
Areas of Frequent Extremes (Tmax)

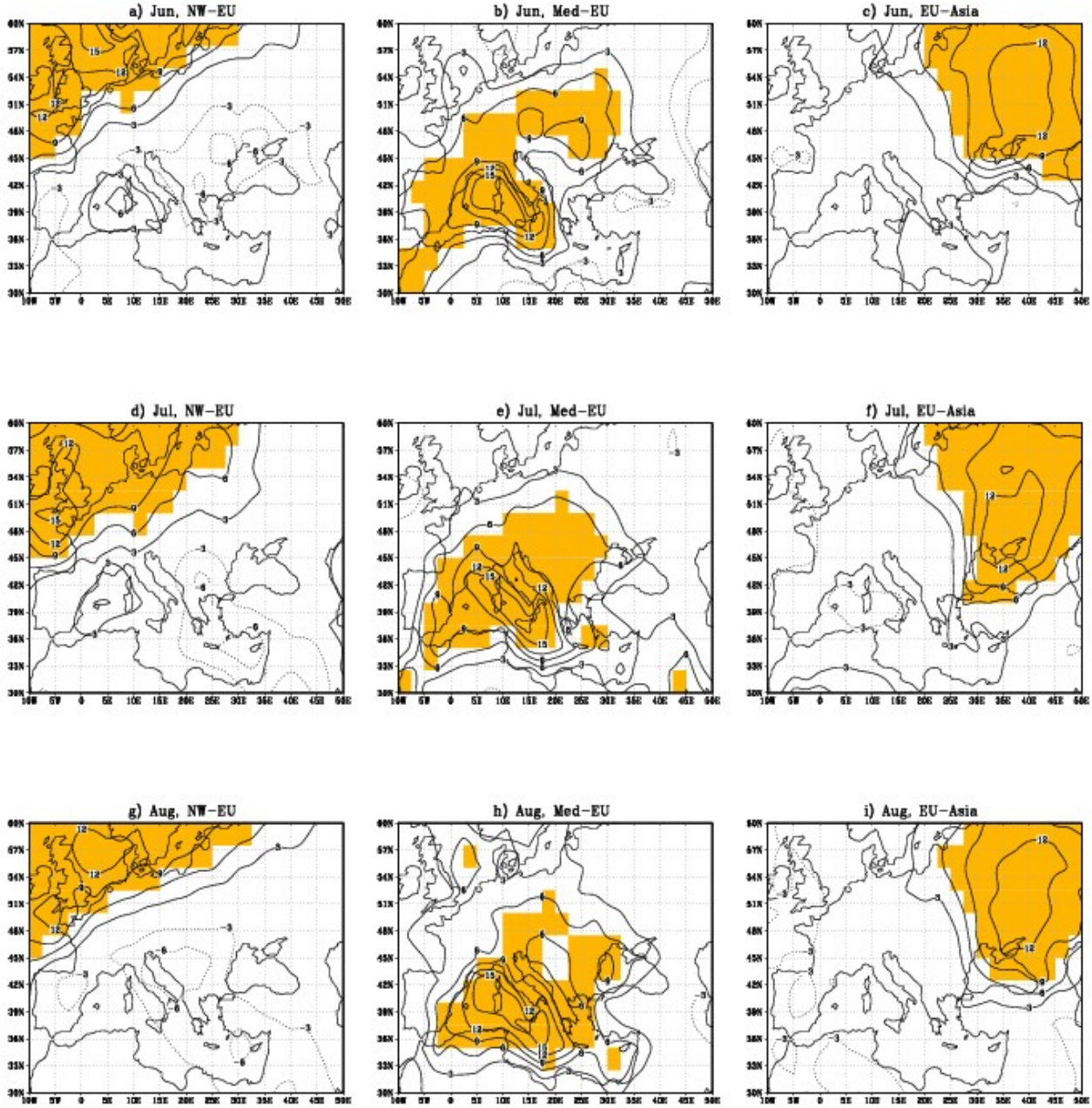

Figure 3, Carril et al., 2007
Anomalies asociated with extremes over NW-EU, June

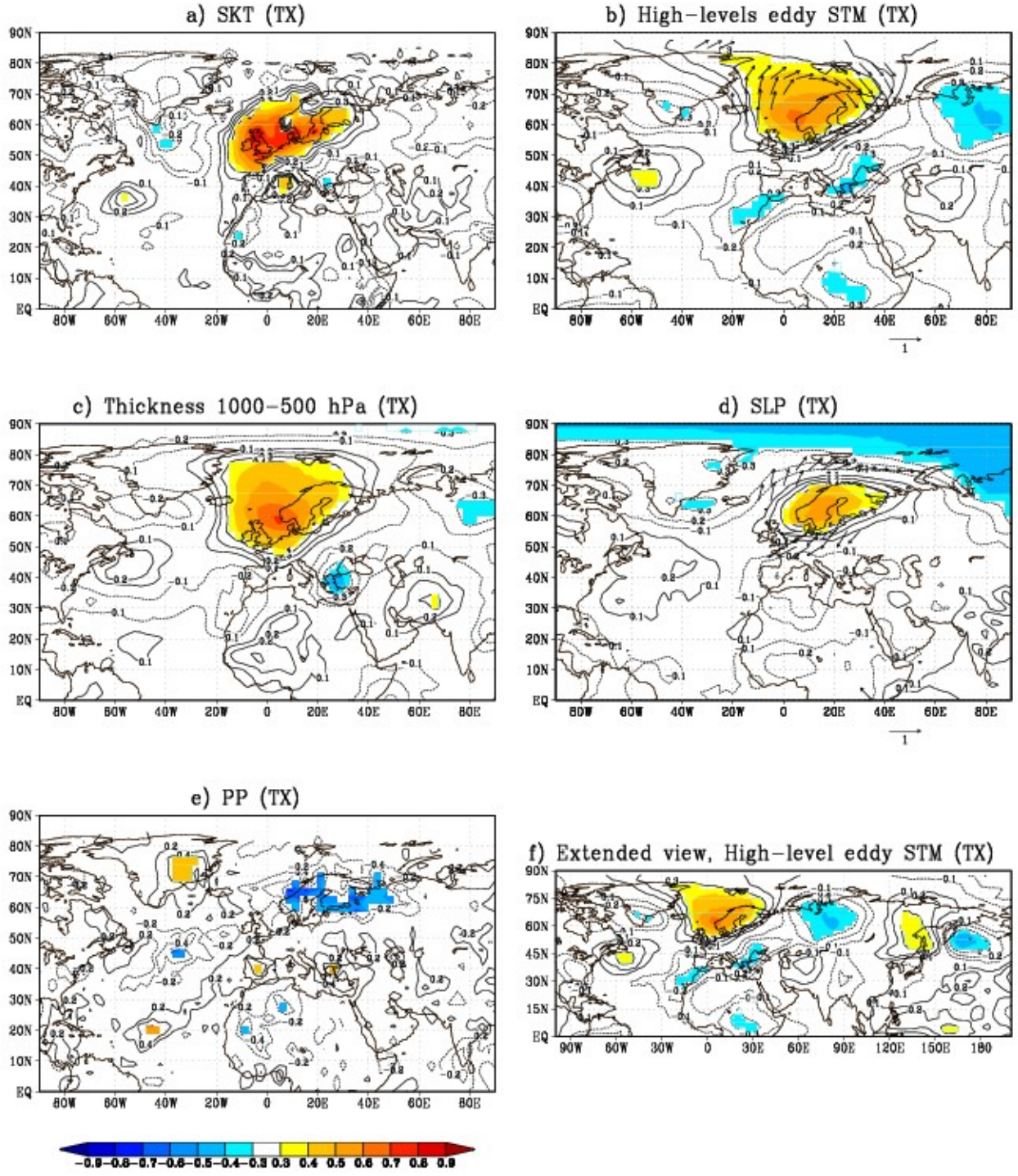

Figure 4, Carril et al., 2007
Anomalies asociated with extremes over NW-EU, July

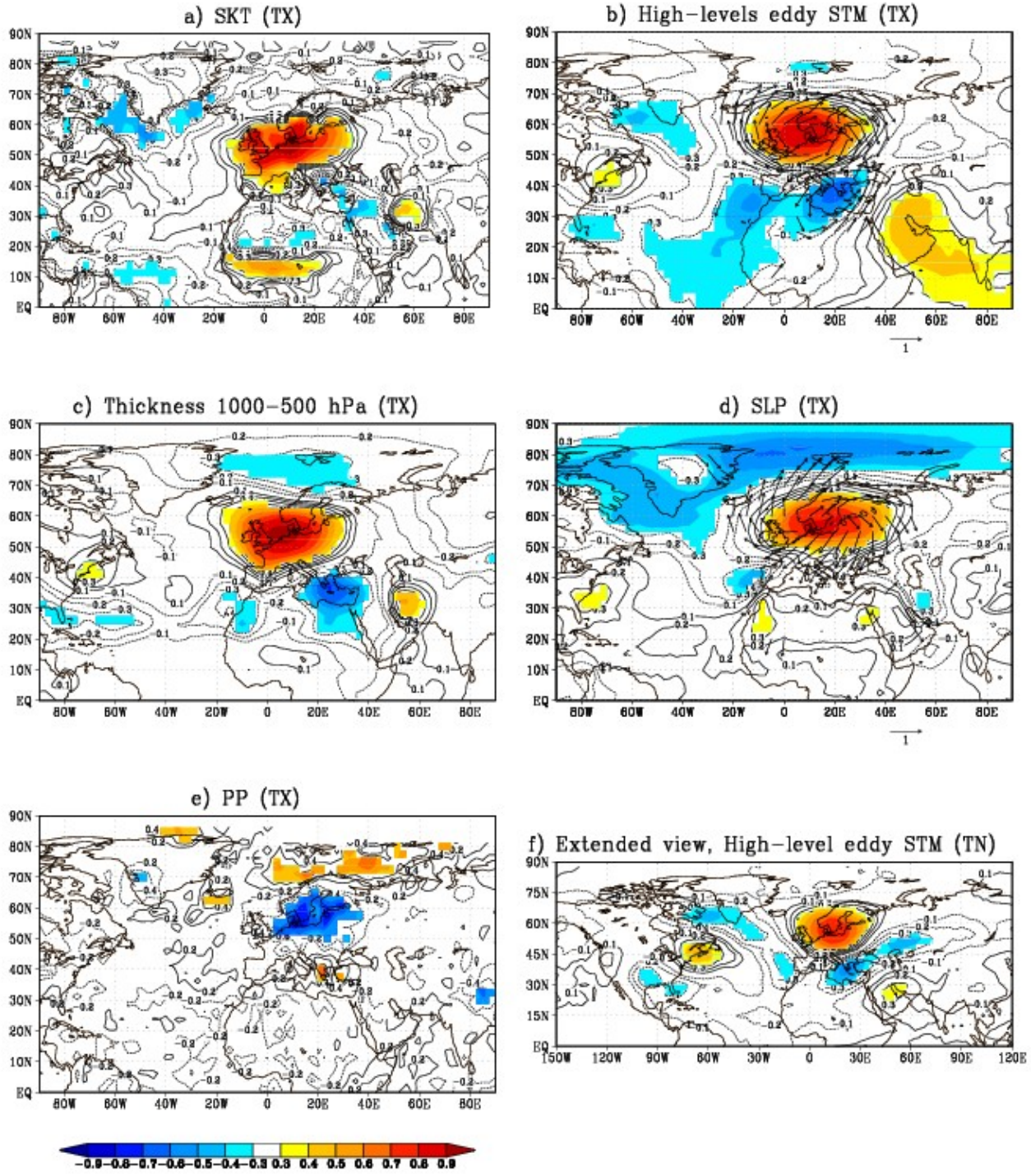

Figure 5, Carril et al., 2007
Anomalies asociated with extremes over NW-EU, Aug

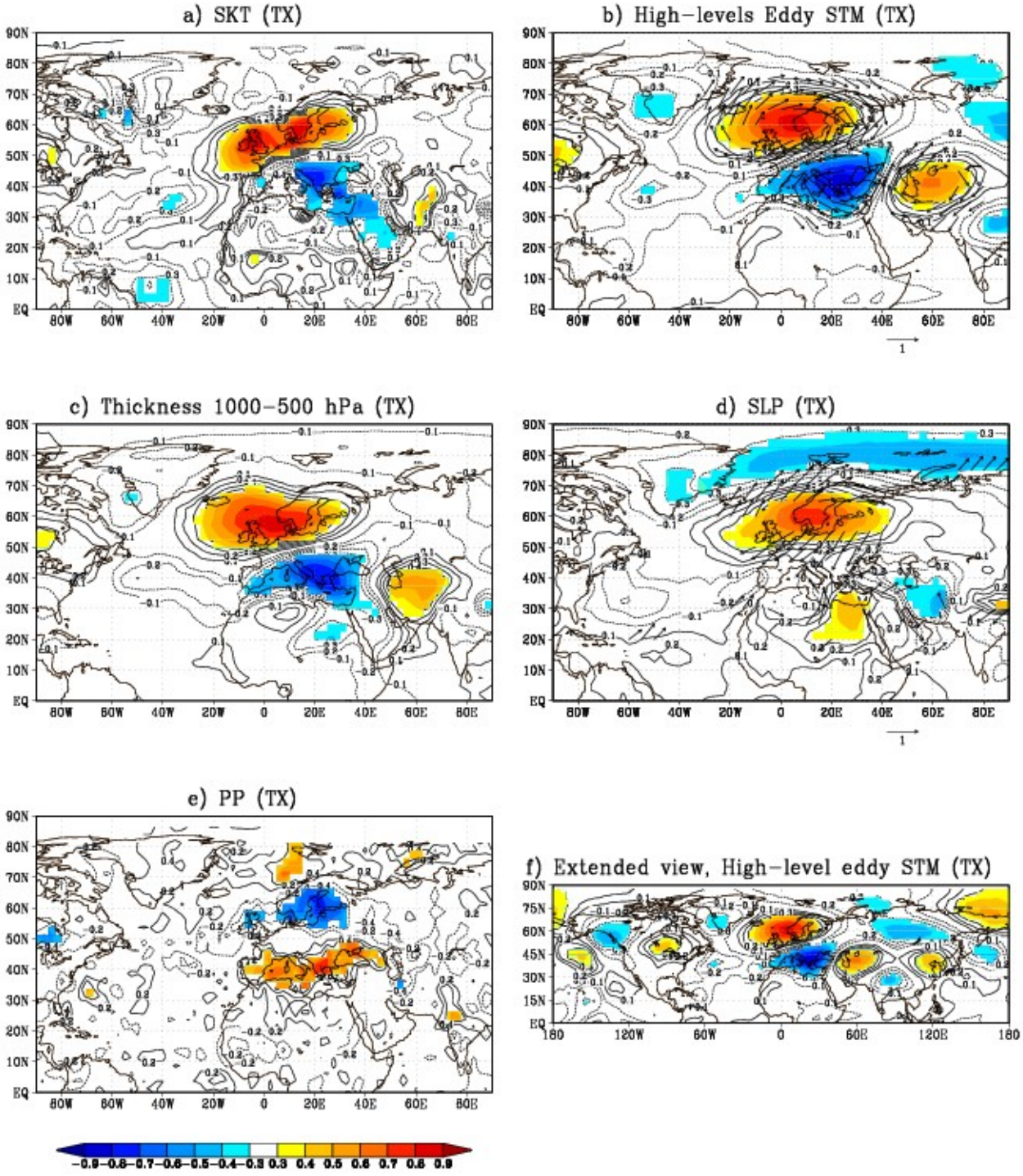

Figure 6, Carril et al., 2007
Anomalies asociated with extremes over Med−EU, June

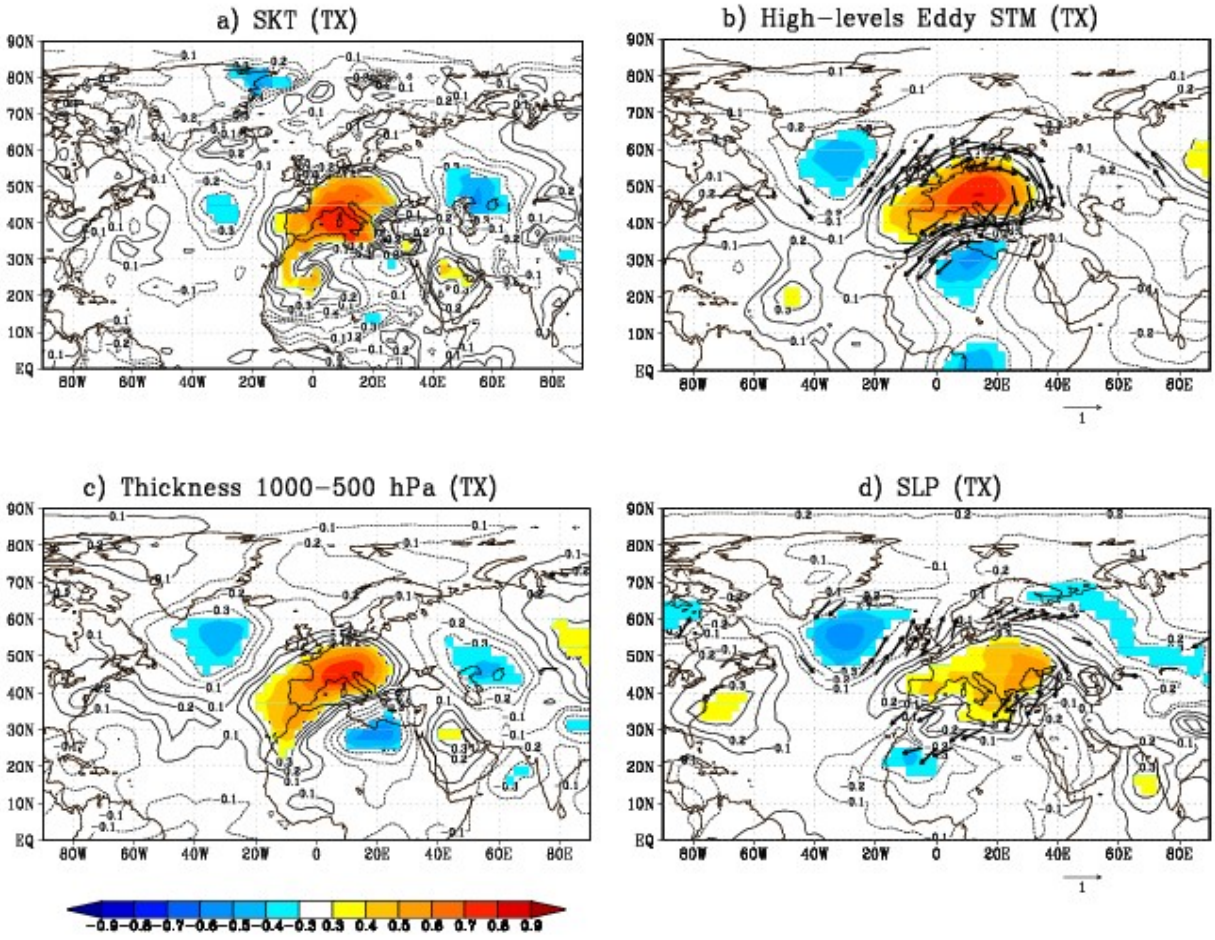

Figure 7, Carril et al., 2007
Anomalies asociated with extremes over Med-EU, July

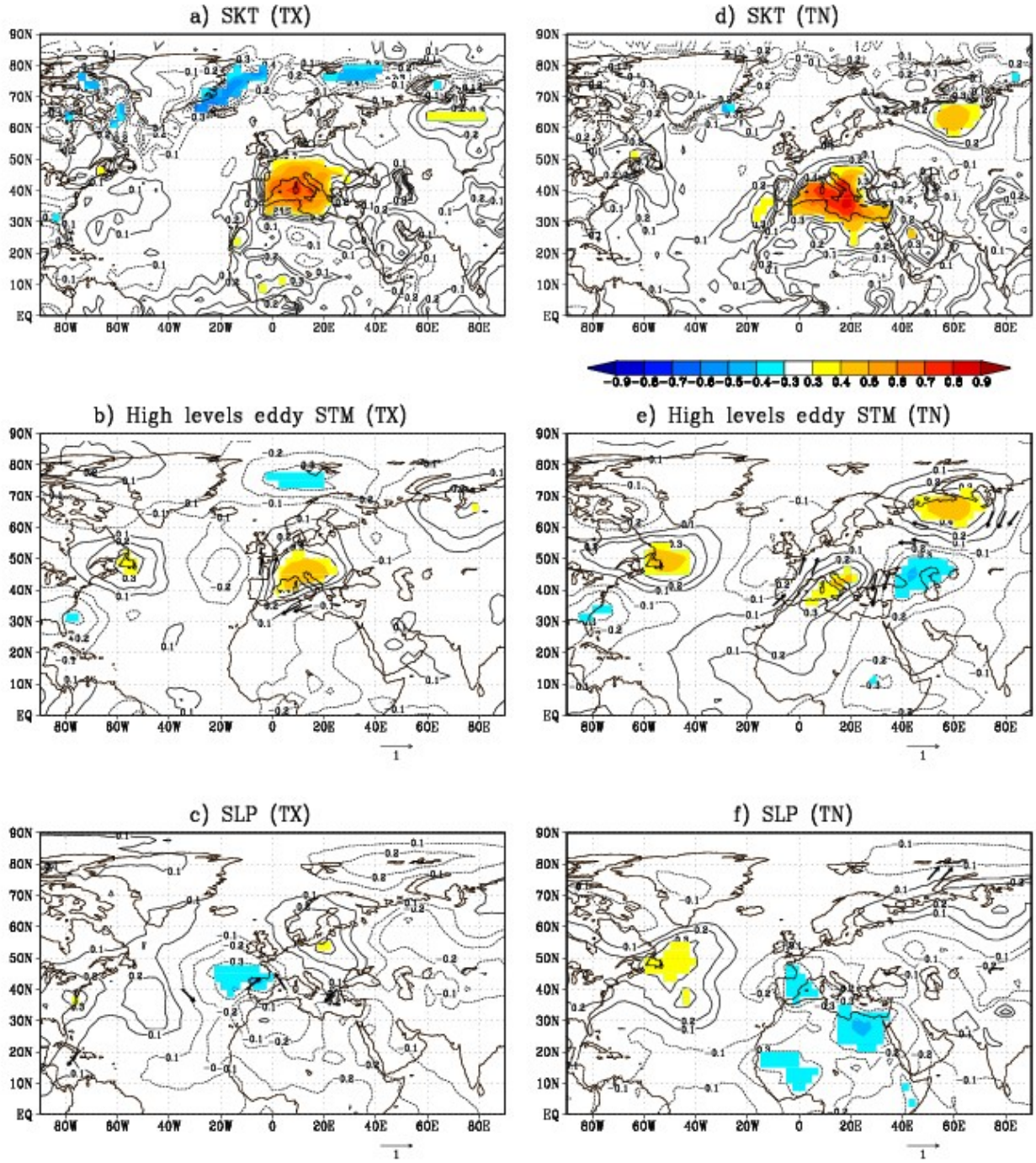

Figure 8, Carril et al., 2007
Anomalies asociated with extremes over Med–EU, Aug.

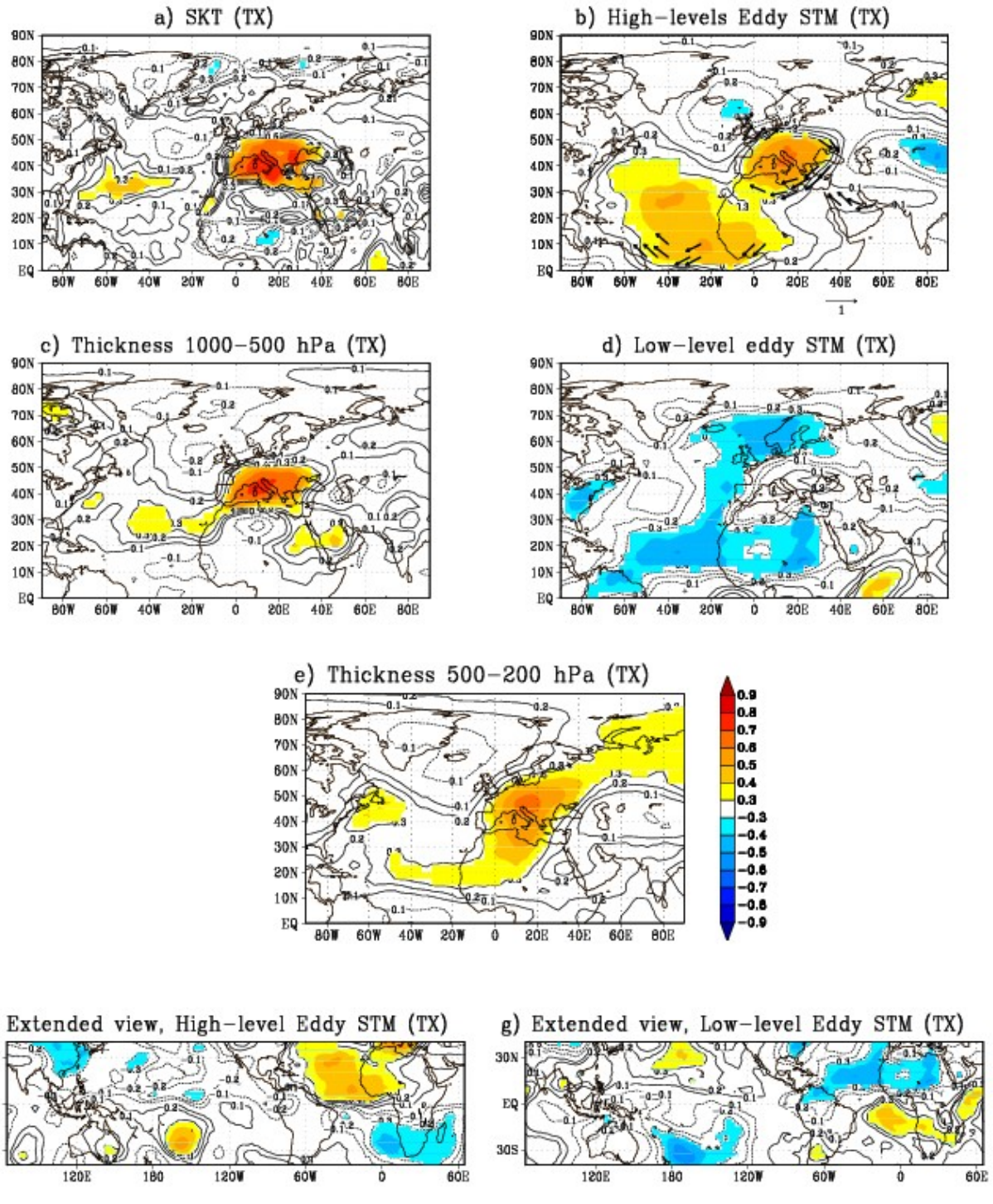

Figure 9, Carril et al., 2007
Anomalies asociated with extremes over EU−Asia, June

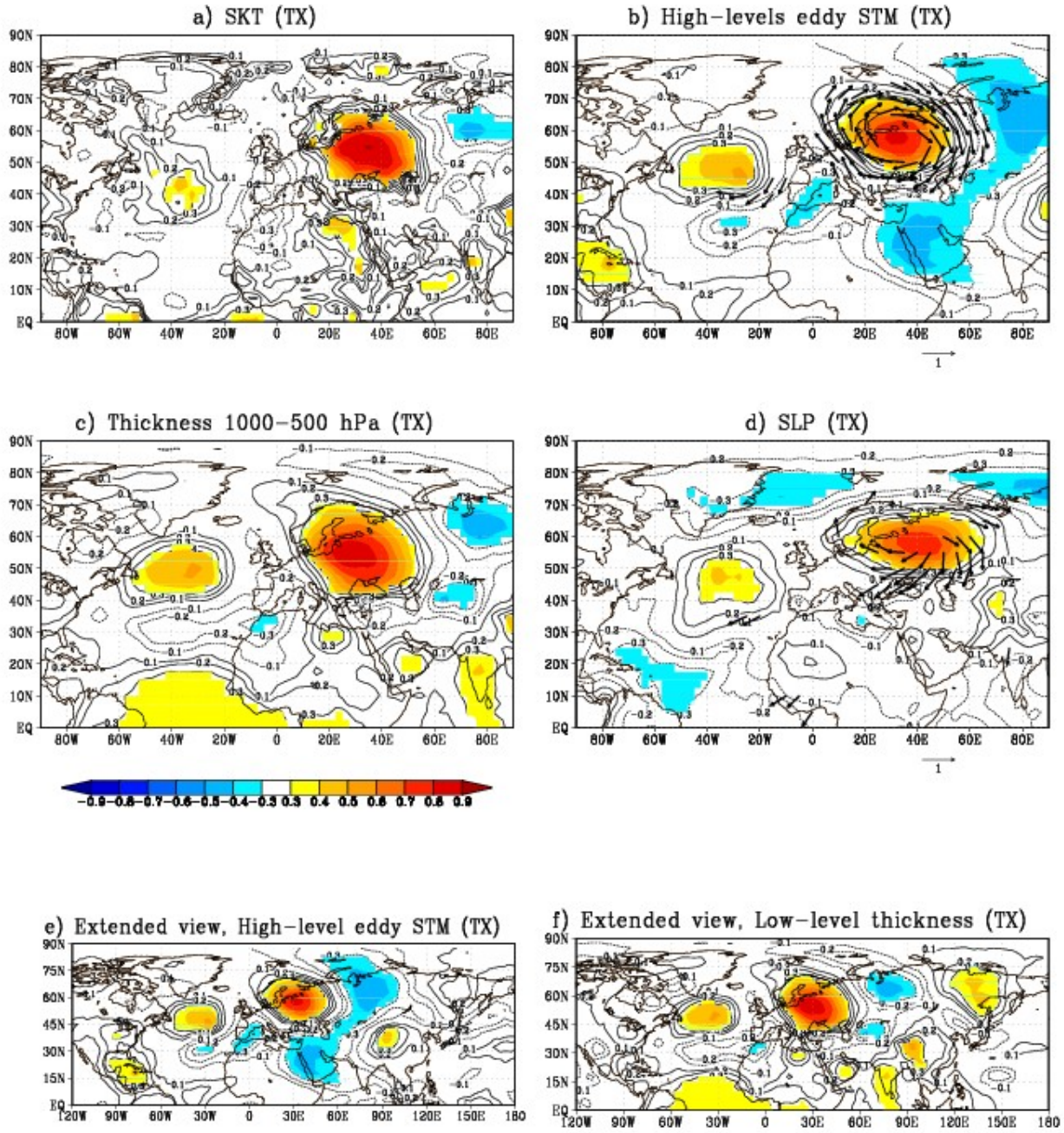

Figure 10, Carril et al., 2007
Anomalies asociated with extremes over EU−Asia, July

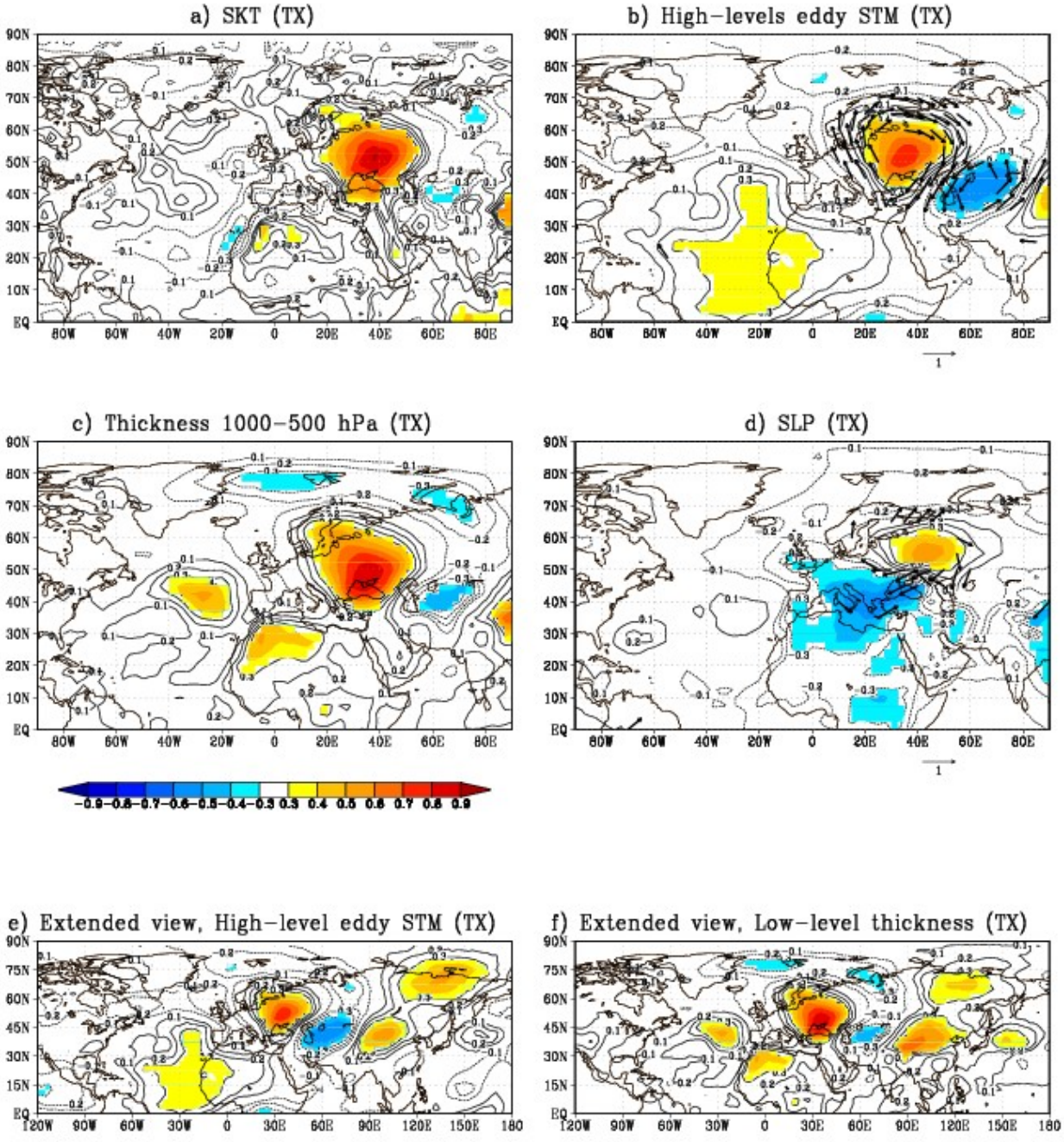

Figure 11, Carril et al., 2007
Anomalies asociated with extremes over EU−Asia, Aug.

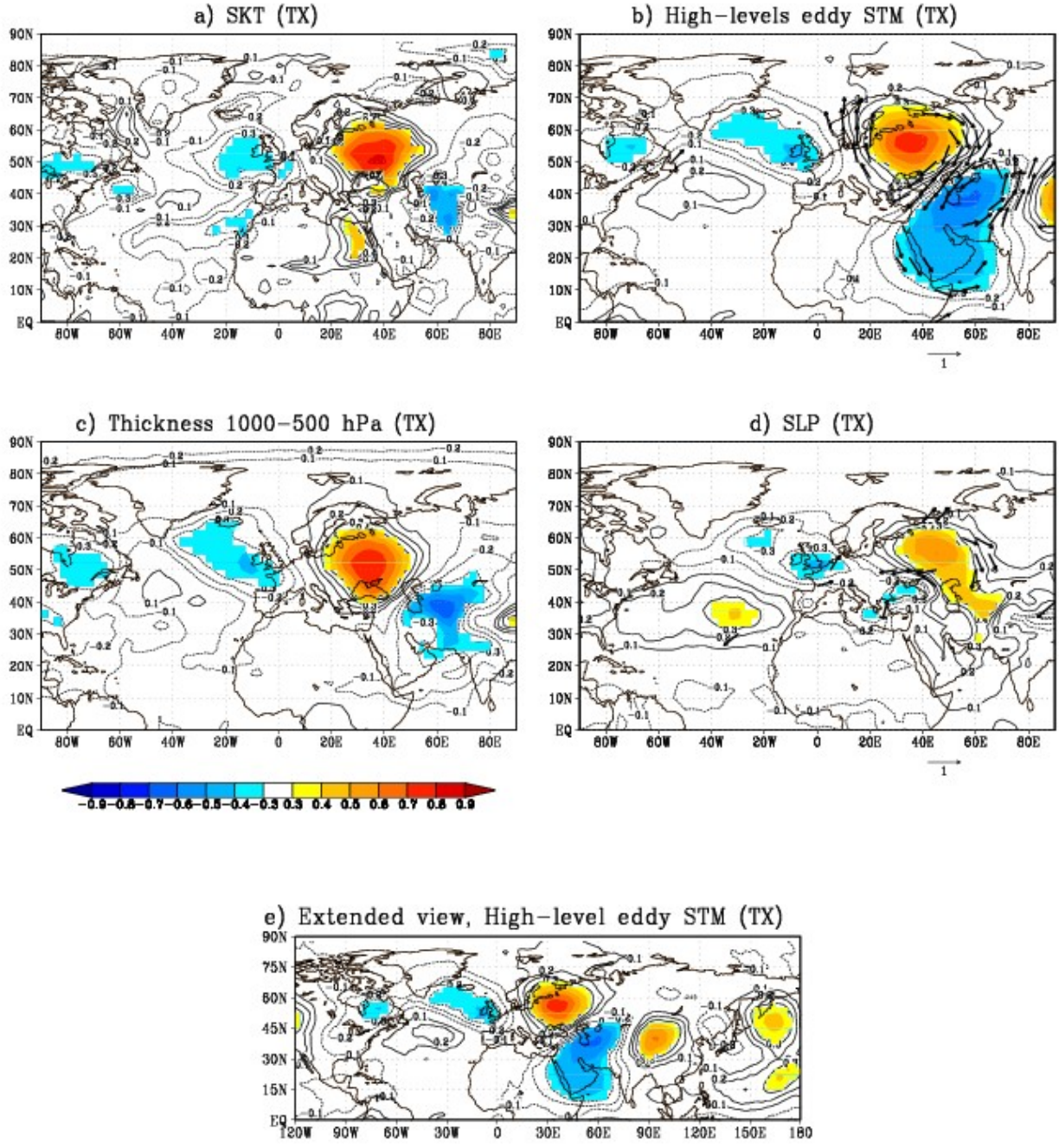

Figure 12, Carril et al., 2007
Reconstruction of 2003

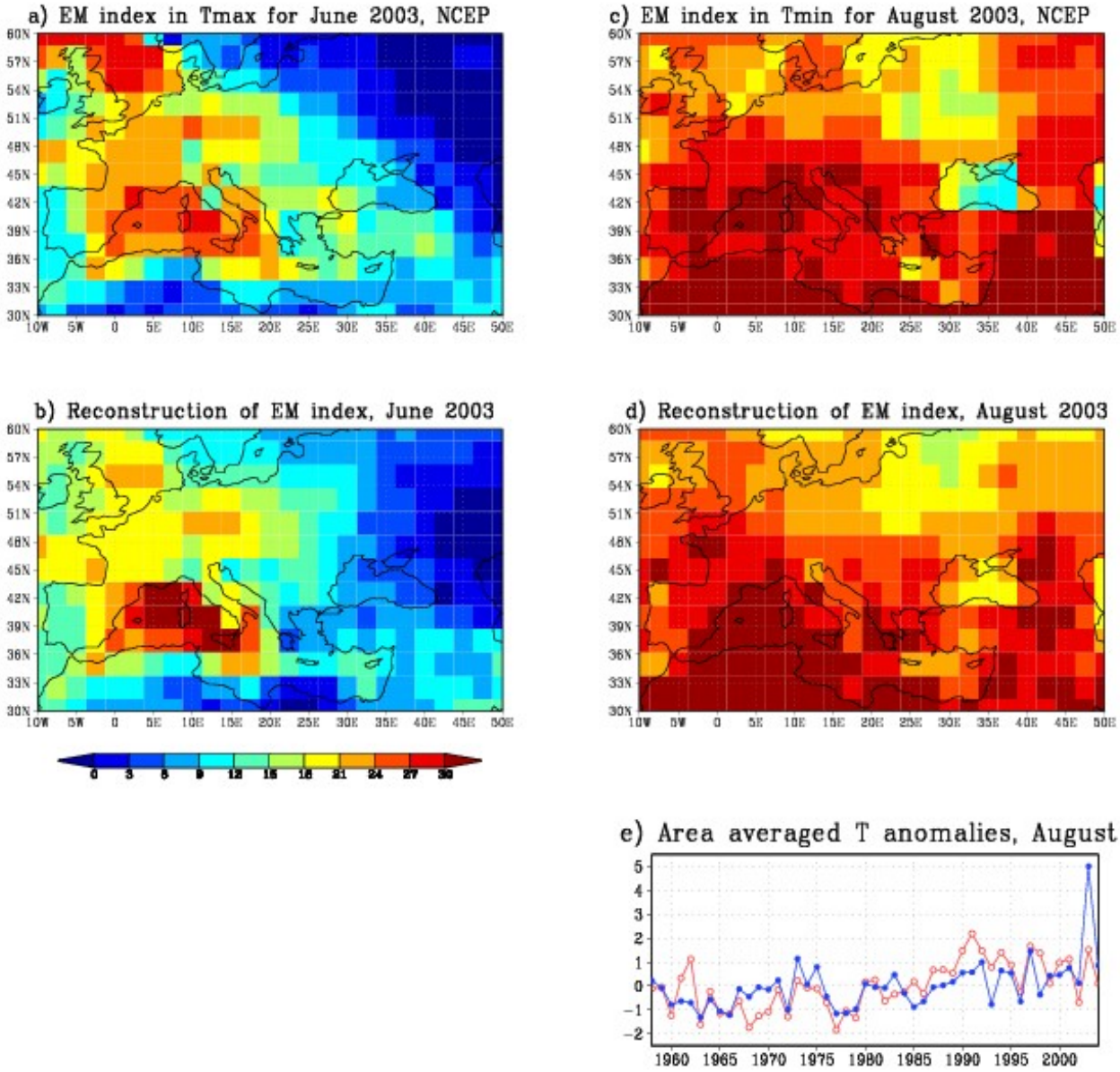

Figure 13, Carril et al., 2007
2003-like composites, June TX

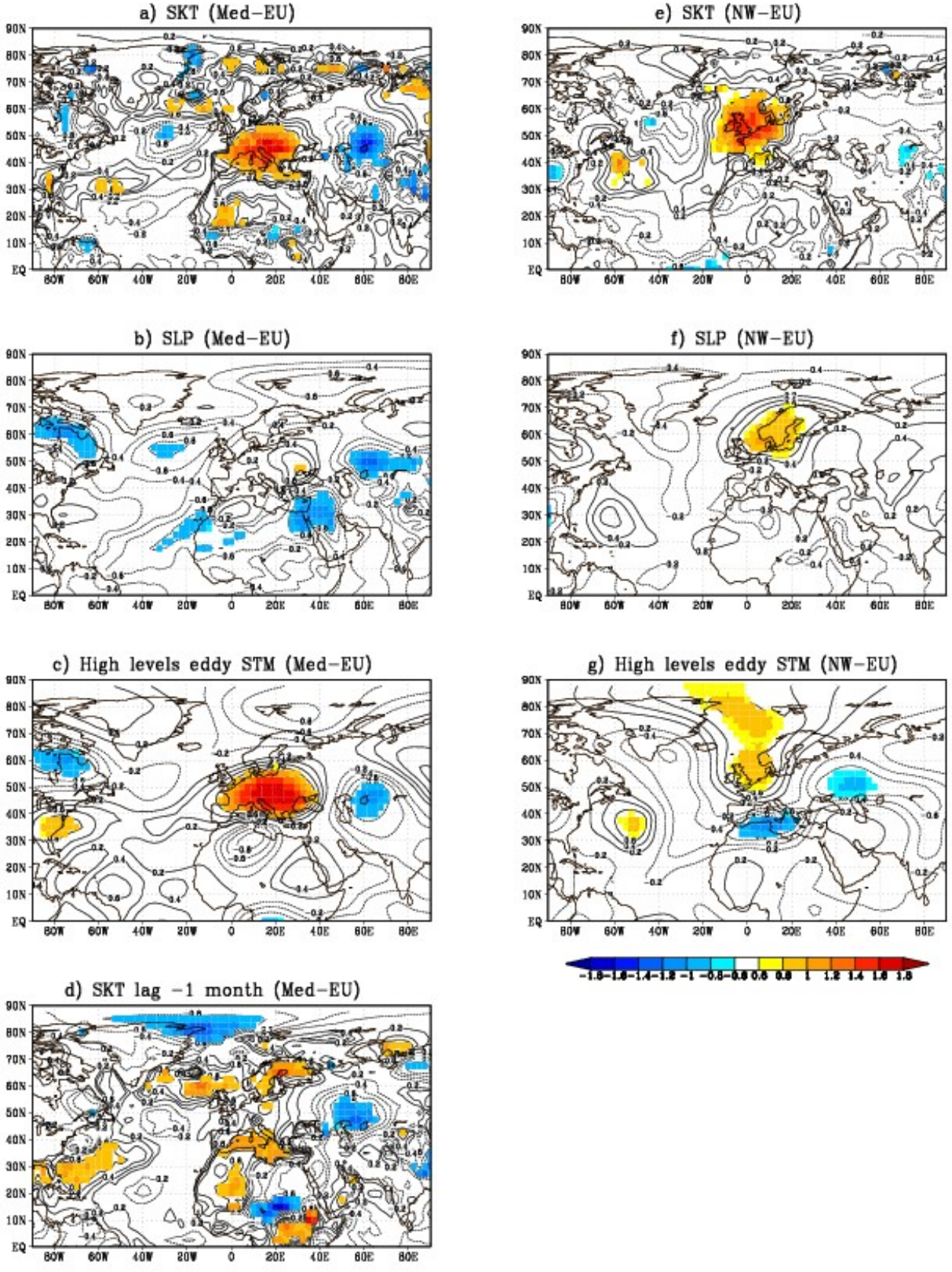

Figure 14, Carril et al., 2007
2003–like composites, Aug TN